

Steady-state properties of a totally asymmetric exclusion process with periodic structure

Greg Lakatos,^{1,*} Tom Chou,^{2,†} and Anatoly Kolomeisky^{3,‡}

¹*Department of Physics, University of British Columbia, Vancouver, British Columbia, Canada V6T-1Z1*

²*Department of Biomathematics, UCLA, Los Angeles, California 90095-1766, USA*

³*Department of Chemistry, Rice University, Houston, Texas, 77251-1892, USA*

(Received 14 October 2003; revised manuscript received 16 August 2004; published 12 January 2005)

We study the steady-state behavior of totally asymmetric simple exclusion processes (TASEPs) that contain periodically varying movement rates. In this model, particles move to the right at one of two rates: p_2 if the particle occupies one of a periodically arranged set of lattice sites; p_1 otherwise. Approximate mean field approaches are used to study the steady-state currents and bulk densities of this model. These mean field methods are found to provide results in good agreement with data derived from Monte Carlo simulations. Finally, the condition for particle-hole symmetry in the TASEP with periodically varying movement rates is specified, and the changes in the locations of the boundary-limited to maximal-current transition lines due to symmetry violation are investigated.

DOI: 10.1103/PhysRevE.71.011103

PACS number(s): 05.60.Cd, 05.70.Ln, 05.10.Gg, 02.50.Ey

I. INTRODUCTION

As a canonical model of one-dimensional transport, the totally asymmetric simple exclusion process (TASEP) is a topic of significant interest. One of the few solvable non-equilibrium models, the TASEP and its solutions have been extensively investigated [1–6,24] as a model for numerous one-dimensional transport processes including ribosome motion [2,7,8], pore transport [10], and traffic flow [11,12]. The traditional TASEP model consists of a finite lattice with open boundaries. Particles are inserted into an empty site at the leftmost end of the lattice at a rate α , while particles in the lattice move to the right at a rate p . Each motion of a particle within the lattice moves that particle exactly one lattice site to the right, and particles can move only if the site immediately to the right is not occupied by another particle. Upon reaching the last lattice site on the right, particles are removed from the lattice at a rate β . Exact solutions for the steady-state particle currents (J), and densities (σ), are available through mean field approaches [1,2], and matrix product methods [3]. The latter approach solves the model completely, providing exact expressions for density correlation functions of arbitrary order. The TASEP solution itself yields a phase diagram with three phases. At large values of the injection (α) and extraction (β) rates the system is dominated by the rate of particle hopping and is in a maximal current phase. At small values of α and β , the system is found in a low-density entry limited phase, and a high-density exit-limited phase, respectively. The fundamental form of this phase diagram has been found to be very robust and extending the TASEP to include particles that occlude more than one lattice site [7,8], or backwards particle motions [9], has not altered the phase diagram significantly. Nonetheless, these extensions have facilitated the use of the TASEP in modeling a wide variety of physical processes.

In many phenomena of interest however, the assumption of a single internal hopping rate p implicit in the normal TASEP does not adequately capture the full character of the transport behavior. Examples include multistep models for molecular motor motion, as well as models of ion transport through transmembrane channels with selectivity filters and solvation zones. Additionally, previous studies of TASEPs with multiple movement rates focused on systems with periodic boundary conditions [13–16], isolated defects [6], or particle associated hopping rates [17], rather than spatially and periodically varying hopping rates with open boundaries.

II. MODEL AND METHODS

To improve the utility of the TASEP in modeling a wider range of systems, we generalize the TASEP to include two internal hopping rates, p_1 and p_2 . Numbering the lattice sites starting from 1 at the far left, we assume the p_2 sites are arranged periodically with a period T (cf. Fig. 1). We apply and compare three mean field approximations to the steady-state current and density of the dual-rate TASEP in the maximal current, entry limited, and exit limited regimes. We also conjecture that the phase diagram of the dual-rate TASEP retains the three phase character of the standard TASEP's phase diagram. The accuracy of our mean field methods are verified through Monte Carlo simulations.

III. MEAN FIELD THEORIES

A. Simple mean field methods

We begin by considering the dual-rate TASEP in the limit of large α and β , where the dynamics of the system will be

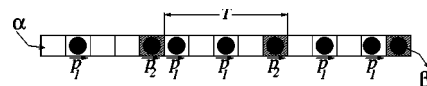


FIG. 1. The periodic dual-rate totally asymmetric exclusion model. At every T lattice site, the particle movement rate is p_2 . At all intervening sites, the movement rate is p_1 . All other aspects of the model are identical to those of the standard TASEP.

*Electronic address: glakatos@physics.ubc.ca

†Electronic address: tomchou@ucla.edu

‡Electronic address: tolya@rice.edu

determined entirely by the internal movement rates p_1 and p_2 . Ensuring continuity of the current in a lattice with periodicity T we find

$$J = p_2 \sigma_T (1 - \sigma_1) = p_1 \sigma_1 (1 - \sigma_2) = \cdots = p_1 \sigma_{T-1} (1 - \sigma_T). \quad (1)$$

In writing Eq. (1) we have assumed that the densities (σ_i) in the lattice have the same period T as the hopping rates in the lattice.¹ Solving Eq. (1) for J in terms of one of the densities σ_i , then maximizing J , yields an approximation to the maximal currents and densities in terms of p_1 and p_2 . Unfortunately, Eq. (1) yields increasingly unwieldy expressions for the current and the densities as T increases. As a result we only show the expressions for the $T=2$ case:

$$\begin{aligned} J &= \frac{p_1 p_2}{(\sqrt{p_1} + \sqrt{p_2})^2}, \\ \sigma_1 &= \frac{\sqrt{p_2}}{\sqrt{p_1} + \sqrt{p_2}}, \\ \sigma_2 &= \frac{\sqrt{p_1}}{\sqrt{p_1} + \sqrt{p_2}}. \end{aligned} \quad (2)$$

These relations show the expected invariance under the interchange of p_1 and p_2 . To find the boundary limited currents in the simple mean field approximation we assume a small value of α or β and assume the lattice contains a whole number of periods, so that the last lattice site is a p_2 site. Focusing initially on the entry-limited case and applying the current continuity conditions we find, for arbitrary T

$$J = \alpha(1 - \sigma_1) = p_1 \sigma_1 (1 - \sigma_2) = \cdots = p_2 \sigma_T (1 - \sigma_1). \quad (3)$$

Yielding the following densities and currents for the $T=2$ case

$$\begin{aligned} J_\alpha &= \alpha(1 - \sigma_1) = p_1 \sigma_1 (1 - \sigma_2) = p_2 \sigma_2 (1 - \sigma_1) \\ \Rightarrow J_\alpha &= \frac{p_1(p_2 - \alpha)\alpha}{p_2(p_1 + \alpha) - \alpha p_1} = \alpha(1 - \sigma_1) \\ \sigma_1 &= \frac{\alpha p_2}{p_2(p_1 + \alpha) - \alpha p_1} \\ \sigma_2 &= \alpha/p_2. \end{aligned} \quad (4)$$

Similarly in the exit limited case we have

$$\begin{aligned} J &= p_2 \sigma_N (1 - \sigma_{N-T+1}) = p_1 \sigma_{N-T+1} (1 - \sigma_{N-T+2}) = \cdots \\ &= p_1 \sigma_{N-1} (1 - \sigma_N) = \beta \sigma_N, \\ J_\beta &= \beta(\sigma_2) = p_1 \sigma_1 (1 - \sigma_2) = p_2 \sigma_2 (1 - \sigma_1) \\ \Rightarrow J_\beta &= \frac{p_1(p_2 - \beta)\beta}{p_2(p_1 + \beta) - \beta p_1} \end{aligned} \quad (5)$$

¹If the instantaneous lattice occupancy is $x_i \in [0, 1]$, the average density at site i in the steady state is defined as $\sigma_i = \langle x_i \rangle$.

$$\sigma_1 = 1 - \frac{\beta}{p_2} \quad (6)$$

$$\sigma_2 = \frac{p_1(p_2 - \beta)}{p_2(p_1 + \beta) - p_1 \beta}.$$

To determine the transitions between the maximal current and entry limited regions we equate the maximal current solutions generated by Eq. (1) to the expressions for J_α and J_β in Eq. (3) and Eq. (5) and solve for the transition values α^* and β^* . For the $T=2$ case this yields

$$\alpha^* = \beta^* = \frac{p_2 \sqrt{p_1}}{\sqrt{p_1} + \sqrt{p_2}}. \quad (7)$$

Finally, equating the current expressions in equations (3) and (5) we find that the transition between the entry and exit limited regions occurs when $\alpha = \beta$.

B. Refined mean field methods

As we will see in the next section, the results of the simple mean field approach do not provide a particularly good match to the results of Monte Carlo (MC) simulations. We attribute the poor performance of the simple mean field method to the method's failure to capture the correlations between the occupation probabilities of different lattice sites. To address this deficiency we apply two related mean field approaches. The first refined mean field approach, which we call the *finite-segment* method (FSMF) [25], involves exactly solving the master equation for a finite segment of the dual-rate TASEP lattice in a self-consistent manner (see Appendix A). While primarily numerical in nature, this method can produce estimates for the current and density comparable to the results from MC simulations. The quality of the estimates produced by the FSMF approach is a function of the length of the finite-segment, with longer segments producing superior results.

The second enhanced mean field method is related to the cluster mean field approach described in [18–20] (see Appendix B). This mean-field method becomes increasingly unwieldy as the size of the cluster increases, thus we only show results for the $T=2$ case. In the maximal current phase the current and density results are

$$\begin{aligned} \sigma_1 &= \frac{p_1 + 2p_2}{3(p_1 + p_2)}, \\ \sigma_2 &= \frac{2p_1 + p_2}{3(p_1 + p_2)}, \\ J &= \frac{p_1 p_2}{2(p_1 + p_2)}. \end{aligned} \quad (8)$$

As expected, the solutions are invariant under the exchange $(\sigma_1, p_1) \leftrightarrow (\sigma_2, p_2)$, and regenerate the standard TASEP results in the limit $p_1 = p_2$.

We can use the results of Eq. (8) to predict the location of the phase boundary between the maximal current and entry

limited phases. Using the results for the densities in the maximal current phase and applying current continuity at the entrance of the lattice we find

$$\alpha^* \left(1 - \frac{p_1 + 2p_2}{3(p_1 + p_2)} \right) = \frac{p_1 p_2}{2(p_1 + p_2)} \Rightarrow \alpha^* = \frac{3p_1 p_2}{2(2p_1 + p_2)}. \quad (9)$$

To find the critical value of the extraction rate β^* , we enforce current continuity at the exit of the lattice

$$\beta^* \frac{2p_1 + p_2}{3(p_1 + p_2)} = \frac{p_1 p_2}{2(p_1 + p_2)} \Rightarrow \beta^* = \frac{3p_1 p_2}{2(2p_1 + p_2)}. \quad (10)$$

Additionally in the $T=2$ case we can use a similar approach (see Appendix B) to find current and density approximations in the parameter regimes where the entry or exit rate limits the rate of particle transport through the lattice. First addressing the entry limited region we find

$$\begin{aligned} J_\alpha &= \frac{\alpha \{ p_1 p_2 - \alpha(p_1 + \alpha) + \sqrt{4p_1^2 \alpha(p_2 - \alpha) + [p_1(p_2 - \alpha) + \alpha^2]^2} \}}{2p_2(p_1 + \alpha)}, \\ \sigma_1 &= \frac{\alpha p_2 + (\alpha + p_1)(\alpha + p_2) - \sqrt{4p_1^2 \alpha(p_2 - \alpha) + [p_1(p_2 - \alpha) + \alpha^2]^2}}{2p_2(p_1 + \alpha)}, \\ \sigma_2 &= \frac{\alpha}{p_2}. \end{aligned} \quad (11)$$

Similarly, the solution in the exit-limited phase is

$$\begin{aligned} J_\beta &= \frac{\beta \{ p_1 p_2 - \beta(p_1 + \beta) + \sqrt{4p_1^2 \beta(p_2 - \beta) + [p_1(p_2 - \beta) + \beta^2]^2} \}}{2p_2(p_1 + \beta)}, \\ \sigma_1 &= 1 - \frac{\beta}{p_2}, \\ \sigma_2 &= \frac{p_1 p_2 - \beta(p_1 + \beta) + \sqrt{4p_1^2 \beta(p_2 - \beta) + [p_1(p_2 - \beta) + \beta^2]^2}}{2p_2(p_1 + \beta)}. \end{aligned} \quad (12)$$

Note that Eqs. (11) and (12) are the analytic forms for the FSMF results for the $T=2$ dual-rate TASEP when the FSMF segment size is set to $N=2$ (see Appendix A).

IV. MONTE CARLO SIMULATIONS

Monte Carlo simulations were performed to validate the various analytical models presented in the preceding section. As we expected the densities in the lattice to vary significantly as the internal hopping rates were varied, we based our Monte Carlo code on the BKL continuous-time algorithm [21]. The BKL algorithm has the advantage of maintaining a constant computational efficiency over a wide range of particle densities.

The magnitude of the finite size effect in our simulations was estimated by running lattices of varying lengths. For lattices one thousand sites long, the MC results were found to systematically deviate from the known TASEP results ($p_1=p_2$) by less than half a percent. As a result, unless otherwise noted we used lattices containing 1000 periods for all our simulations. The simulations were run for 7×10^8 steps, which was sufficient to reproduce the known TASEP results in lattices much longer than our 1000 period standard. In all

simulations, p_1 was normalized to 1. To ensure an unbiased sampling of the lattice states, a linear-congruential pseudo-random number generator with a period of 2×10^{18} was used [22].

A. Currents

The maximal current results [Fig. 2(a)] show the expected qualitative behavior with a low current for small values of p_2 and a value of $1/4$ when $p_2=p_1=1$. In Fig. 2(a) the boundary-limited current predictions [Eq. (11)] were used to generate a prediction for the maximal current as a function of p_2 . This was accomplished by maximizing J in Eq. (11) with respect to α . Consistent with our expectations, we find that the two cluster mean field approaches, and the finite-segment mean field approach, provide better approximations to the Monte Carlo results than does the simplest mean-field method. The relatively poor performance of the simple mean field model can be ascribed to the pair correlations present in the two-rate TASEP, which the simple mean field model completely fails to capture. The 2-cluster maximal current mean field clearly performs best when $p_2/p_1 \approx 1$. In this limit the model is essentially the normal single rate TASEP, and

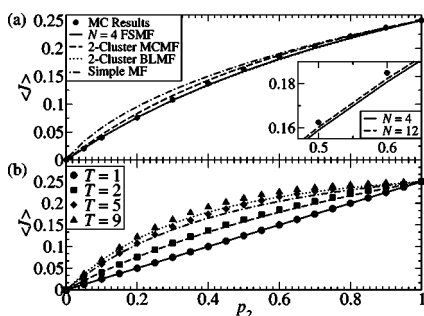


FIG. 2. (a) The Monte Carlo (MC), $N=4$ finite-segment mean field (FSMF), 2-cluster maximal current mean field (MCMF), 2-cluster boundary limited mean field (BLMF), and the simple mean field predictions for the $T=2$ TASEP current in the maximal current phase. The results for the 2-cluster boundary limited mean field method were produced by maximizing J in Eq. (11). The estimates of the $N=4$ FSMF and the 2-cluster BLMF approach are nearly identical. Inset: The effect of increasing segment length on the quality of the FSMF estimates. For segment lengths greater than or equal to twice the period, the quality of the current estimate shows only marginal improvement with increasing segment length. (b) Maximal currents for dual-rate TASEPs of various periods. The FSMF estimates were produced using a single period of the lattice as the finite segment. While providing reasonable estimates, the deviation between the MC (points) and FSMF (lines) results increases as the period (T) increases. This increase in error can be partially mitigated by increasing the number of periods included in the finite segment.

the expected pair correlations between adjacent p_1 and p_2 sites are small. (See Fig. 3.)

B. Densities

Referring to Figs. 4–6, we find the finite-segment mean field, and both 2-cluster mean field methods provide excellent matches to the simulation results. The densities produced by the maximal current 2-cluster mean field method, the boundary limited 2-cluster mean field method, and the finite segment method are all within 5% of the MC results,

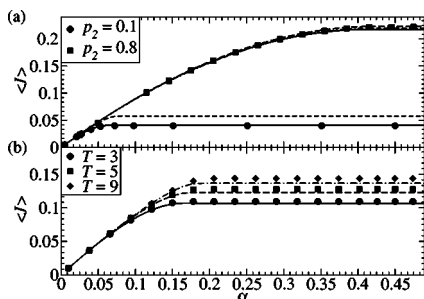


FIG. 3. (a) Current profiles along the α direction in the $T=2$ dual-rate TASEP phase plane. The solid lines were produced using Eq. (11), the dashed lines were produced using Eq. (4), and the dotted-dashed lines were produced using an $N=8$ FSMF approach. Equation (11) and the FSMF approximation are nearly identical. (b) Current profiles for dual-rate TASEPs of various periods with $p_2=0.25$. The FSMF results (lines) were produced using an $N=T$ FSMF approach.

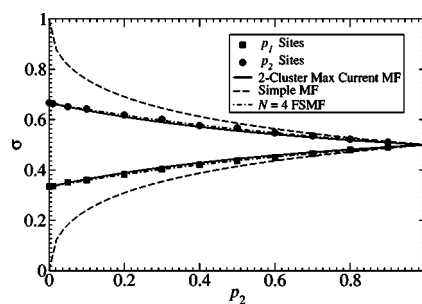


FIG. 4. Densities for a $T=2$ TASEP from Monte Carlo simulations, the 2-cluster maximal current mean field method, the simple mean field method, and an $N=4$ finite segment mean field approach. The simple mean field assumption results in the largest error for small values of p_2 where the density correlation between adjacent sites is expected to be large.

with the FSMF results improving with increased segment length. For all three approaches the quality of the agreement is relatively uniform over all the values of p_2 . Figure 5 displays the density profile in the center of the lattice for TASEPs with $T=5$ and $T=9$. Far from the boundaries, the density profiles show the expected periodicity in all three phases.

C. Correlations

Defining the density correlation function for sites i and j as

$$r_{x_i, x_j} = \frac{\langle x_i x_j \rangle}{\langle x_i \rangle \langle x_j \rangle} - 1, \tag{13}$$

Fig. 7(a), shows that in the maximal current phase in the $T=2$ case, the pair correlation is large for small values of p_2 while approaching zero as p_2 approaches p_1 . The size of this pair correlation for small p_2 indicates that the slow sites dominate the dynamics of the system, and is consistent with the maximal current assumption.

Figure 7(b) displays the the density correlation between the p_2 sites and the p_1 sites immediately to the right in the maximal current phase. The anticorrelation that occurs at longer periods can be explained if we consider the density

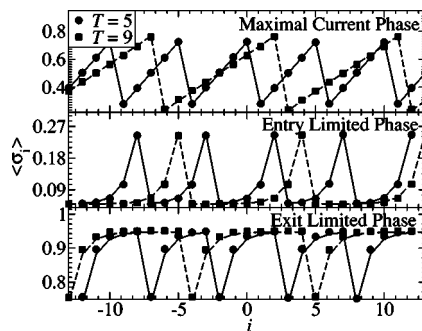


FIG. 5. The bulk density profiles for the $T=5$ and $T=9$ dual-rate TASEPs with $p_2=0.2$, in all three current phases. The plots show the good agreement between the Monte Carlo (points) and $N=T$ FSMF (lines) results.

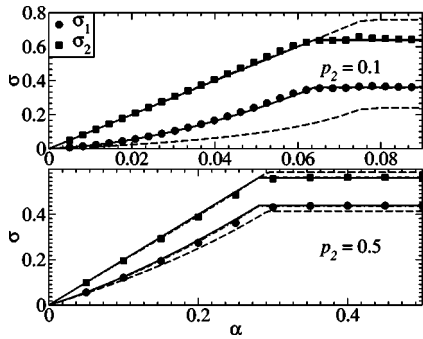


FIG. 6. The density profile along the α direction in the $T=2$ dual-rate TASEP phase plane. The solid lines were produced using Eq. (11), the dashed lines were produced using Eq. (4), while the dotted-dashed lines were produced by an $N=8$ finite-segment mean field approach. The FSMF results are nearly identical to those of Eq. (11). Although the solution for σ_2 is the same in Eqs. (4) and (11), the predicted value of α^* differs between the two mean field theories. This is the reason for the significant difference between the σ_2 profiles predicted by the two mean field methods at small values of p_2 .

profiles of Fig. 5. Focusing on a single period in the center of the lattice, for large T the density of the first few lattice sites in a period should be relatively low. This is a result of the slow rate of particle injection from the p_2 site immediately left of the period, and due to the relatively large value of T that prevents particles from backing-up due to the slow exit rate from the period. As a result of this density profile, the lattice site immediately to the right of a p_2 site would typically only be filled for a short time after leaving the now empty p_2 site, leading to the observed anticorrelation. Comparing the predictions of the finite-segment mean field method for the growth in the anticorrelation with increasing T , it's clear the FSMF underestimates this effect. As a result we would expect that, for segments incorporating a fixed number of periods, the predictions of the FSMF method would become progressively worse as T is increased. Additionally as the FSMF would over-estimate the degree of particle blocking at the period boundaries, we would expect the FSMF method to in general underestimate the current with

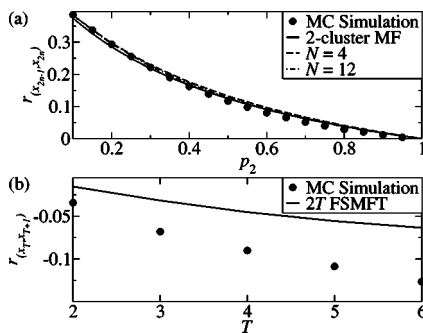


FIG. 7. (a) The maximal current phase pair correlation function produced by the MC simulations and the various mean field approximations for the $T=2$ dual-rate TASEP. The results produced by the finite segment mean field method improve with an increasing segment length. (b) Mean density correlations between $p_2=0.5$ sites and the p_1 sites immediately to the right.

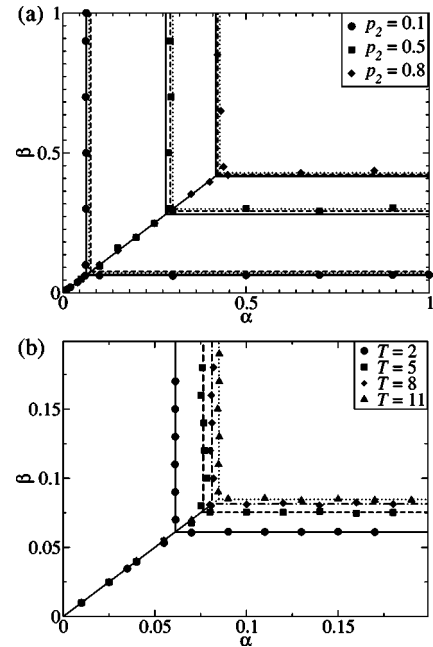


FIG. 8. (a) The phase diagram for the $T=2$ two-rate TASEP. The dashed lines are produced by the simple mean field theory [Eqs. (4) and (6)]. The dotted lines are produced by the maximal current 2-cluster method [Eqs. (9) and (10)] and the solid lines are produced by the boundary-limited mean field method [Eqs. (11) and (12)]. (b) The phase diagram for the two-rate TASEP at various periodicities, with $p_2=0.1$. To simulation accuracy the transition between the high and low density phases occurred along the $\alpha=\beta$ line for all the periodicities displayed.

increasing T , as is confirmed by the results of Fig. 2(b). The degradation in performance of the FSMF method with increasing T can be partially offset by increasing the number of periods in the finite segment, however the rapid increase in computational cost with increased segment length limits the effectiveness of this approach.

D. Phase diagram

The phase diagram derived from simulations is displayed in Fig. 8(a) for the $T=2$ case, along with the phase boundaries predicted by the various mean field methods. The Monte Carlo phase boundaries were computed by taking numerical derivatives of the mean value of σ_2 in the central half of the lattice as a function of α and β , and locating any clear discontinuities in the derivatives. The dual-rate TASEP retains the general form of the standard TASEP phase diagram, and the order of the transitions remains unchanged; first order in the current between the high and low density regimes, and second order between the boundary limited and maximal current regions. The most significant deviation from the standard phase diagram is the increase in the maximal current region which accompanies a decrease in one of the hopping rates (p_2 in our example). Physically, the maximal current region is defined as the region of the (α, β) parameter space where the internal motions determine the net particle flow through the lattice. The increase in the area of the maximal current phase with decreasing p_2 is then expected, as

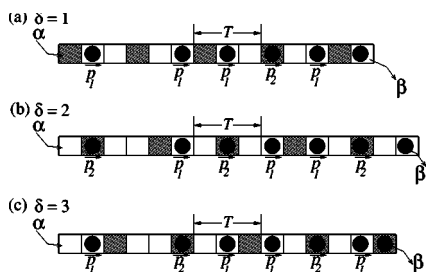


FIG. 9. Variations on the periodic dual-rate TASEP. The three lattices displayed correspond to (a) $\delta=1$, (b) $\delta=2$, and (c) $\delta=3$. In each case the lattice length was chosen to ensure that the resulting TASEP possessed particle-hole symmetry.

decreasing p_2 slows the motion of the particles in the interior of the lattice.

Despite the varying degrees of success in predicting accurate steady state currents and densities, all three mean field approaches predict the phase boundaries within approximately 20% error. As was observed in the mean field predictions for the steady state currents and densities, the boundary-limited 2-cluster mean field approach provides the best predictions at small values of p_2 , while the maximal current mean field method excels when $p_2 \approx p_1$. We also note that the phase transitions predicted by the boundary-limited 2-cluster approach were determined numerically by maximizing J in Eq. (11) and (12). Figure 8(b) displays the change in the phase diagram as the period T is increased and $p_2=0.1$ is held constant. The major effect of increasing T at a fixed p_2 is to increase the values of $\alpha^* = \beta^*$. This is consistent with Fig. 7(b) which shows an increasing anti-correlation with increased T . With an anti-correlation at the period boundaries, particle blocking in the interior of the lattice would be reduced and the values of α or β at which the internal movements of the particles would become the rate limiting step would increase.

V. OTHER PERIODIC ARRANGEMENTS

The dual-rate TASEP model investigated in the previous sections was built on lattices composed of an integer number of $\{p_1, p_1, p_1, \dots, p_2\}$ periods. While a useful extension to the TASEP, it is also interesting to investigate other periodic arrangements of defect sites. For example we can consider the case where the first defect is located at an arbitrary site δ within the first T sites of the lattice, as well as lattices that do not contain a whole number of periods (cf. Fig. 9). When considering these variations on the dual-rate TASEP model however, the issue of particle-hole symmetry arises.

To investigate the conditions under which a periodic dual-rate TASEP would preserve particle-hole symmetry, first define a vector \vec{r} consisting of all the movement rates in the TASEP lattice. Specifically, \vec{r} is constructed so that element r_i gives the rate at which particles in lattice site i move to the right. Additionally, N is defined to be the total length of the TASEP lattice. Now consider the probability $P(\alpha, \beta, \vec{r}, x_1, x_2, \dots, x_N)$ of finding the TASEP lattice in an occupancy state x_1, x_2, \dots, x_N with injection rate α , extrac-

tion rate β , and hopping rates \vec{r} . Here $x_i=1$ if lattice site i is occupied, $x_i=0$ otherwise. Particle-hole symmetry then requires

$$P(\alpha, \beta, \vec{r}, \{x_1, x_2, \dots, x_N\}) = P(\beta, \alpha, \vec{r}, \{\bar{x}_N, \bar{x}_{N-1}, \dots, \bar{x}_1\}), \quad (14)$$

where $\bar{x}_i=0$ if $x_i=1$, and $\bar{x}_i=1$ if $x_i=0$. For Eq. (14) to hold, the rate of the particle movement that takes the TASEP lattice from a occupancy state $i=\{x_1, x_2, \dots, x_N\}$ to an occupancy state j must equal the rate of the particle movement that takes the lattice from state $\bar{i}=\{\bar{x}_N, \bar{x}_{N-1}, \dots, \bar{x}_1\}$ to occupancy state \bar{j} . This places constraints on the possible values of N that can produce particle-hole symmetry.

To determine the symmetry-preserving values of N , consider a lattice occupancy state i where a particle located at site k moves to site $k+1$, changing the lattice state to j . By definition this movement would occur at rate r_k . In lattice state \bar{i} the equivalent move involves a particle hopping from site $N-k$ to site $N-(k-1)$ at a rate r_{N-k} . The definition of the particle-hole symmetry operation [Eq. (14)] ensures that the final state is then \bar{j} . To have these exchange-symmetric moves occur at the same rate, r_k must equal r_{N-k} . Now consider the case where $r_k=p_2$. Then by definition of the dual rate TASEP, $k=mT+\delta$ for some integer m (see Fig. 9). Particle hole-symmetry will then be satisfied if

$$N - mT - \delta = nT + \delta \Rightarrow N = (n+m)T + 2\delta \quad (15)$$

for an arbitrary integer n . Thus the dual-rate TASEP model can only satisfy particle-hole symmetry when $N=sT+2\delta$ for some integer $s \geq 1$. Geometrically, satisfying Eq. (15) guarantees that if the first defect is located at site δ of the lattice, the last defect will be located at lattice site $N-\delta$.

To see that a value of N satisfying Eq. (15) will never confuse particle movements occurring at rate p_1 for those occurring at rate p_2 , consider the case when $k=mT+\gamma$ where $\gamma \leq T$, $\gamma \neq \delta$. Then under symmetry exchange, a particle move occurring at rate r_k would be mapped to a move occurring at rate

$$r_{N-k} = r_{(s-m)T+\delta+(\delta-\gamma)}. \quad (16)$$

As $\gamma, \delta \leq T$ and $\gamma \neq \delta$, there are no integers m, n, s such that $(s-m)T+\delta+(\delta-\gamma)=nT+\delta$. Thus a particle movement occurring at a rate p_1 cannot be mapped to a movement occurring at rate p_2 under the symmetry exchange operation. An interesting consequence of the restriction on N is that a lattice with the first p_2 site located at site T and containing a whole number of periods preserves symmetry regardless of the value of T , while a lattice with the first p_2 site at lattice site 1 and containing a whole number of periods violates symmetry if $T \neq 2$.

Figure 10(a) shows the phase diagrams for various symmetric and non-symmetric realizations of the dual-rate TASEP with $T=3$. From Fig. 10(a) it is clear that violations of condition (15) produce a phase diagram that does not preserve the symmetry about the $\alpha=\beta$ line that is found in standard TASEP phase diagram. Conversely, when condition (15) is satisfied, this symmetry reappears. Note that, within

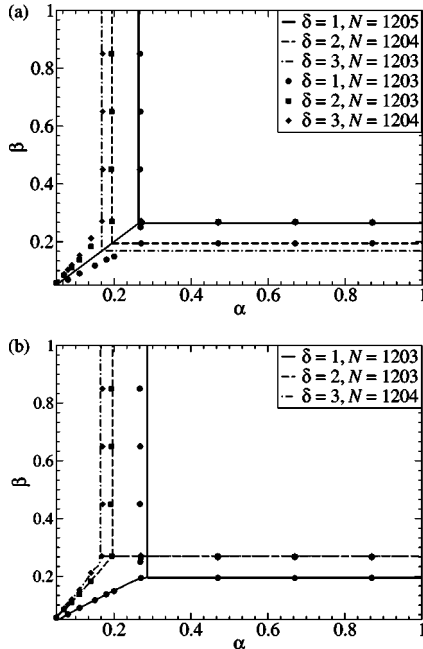


FIG. 10. (a) Phase diagrams for the $T=3$ dual-rate TASEP for various values of δ and N derived from Monte Carlo simulations. The lines are the best-fit phase boundaries for TASEPs with values of N that satisfy Eq. (15). The points are the Monte Carlo predictions for the phase boundaries of TASEPs with values of N that violate Eq. (15). Note that in both the $(\delta=1, N=1203)$ TASEP and the $(\delta=2, N=1204)$ TASEP the last defect is located at lattice site $N-2$ and the TASEP share a common value for β^* . Additionally, TASEPs $(\delta=2, N=1203)$, $(\delta=3, N=1204)$, and $(\delta=1, N=1205)$ all share a common location for the last defect site, and share a common value of β^* . (b) A comparison of the Monte Carlo (points) and finite-segment mean field (lines) predictions for the phase boundaries of various $T=3$ TASEPs that violate particle-hole symmetry. The FSMF predictions were generated using segments that were $3+\delta$ sites long.

simulation accuracy, the phase diagrams of the nonsymmetric dual-rate TASEPs retain the general three phase form the standard TASEP phase diagram for all values of δ and N tested.

The values of α^* and β^* for the nonsymmetric phase diagrams of Fig. 10(a) suggest that the location of the first defect site determines the value of α^* , while the location of the last defect site independently determines the value of β^* . For example, consider the $T=3$ case with $(\delta=1, N=1203)$ where $\alpha^* \approx 0.27$ and $\beta^* \approx 0.19$. By construction, this realization of the $T=3$ dual-rate TASEP and the symmetric version of the $T=3$ dual-rate TASEP with $(\delta=1, N=1205)$ both place the first defect at lattice site 1. The two realizations of the TASEP then share the same value for α^* (≈ 0.27). Conversely, the nonsymmetric $(\delta=1, N=1203)$ case and the symmetric $(\delta=2, N=1204)$ case both have the last defect in lattice site $N-2$, and share the same value of $\beta^* \approx 0.19$. This pattern held for all values of δ and N examined.

Finally we note that mean field methods similar to those worked out in detail for the $\delta=T$ case can be applied to both symmetric and nonsymmetric cases independent of the value of δ . As can be seen in Fig. 10(b), the finite-segment mean

field method provides reasonably accurate estimates for the phase boundaries in all three nonsymmetric cases displayed. We note however that the convergence properties of the finite segment method are most advantageous in the $\delta=T$ case.

VI. CONCLUSION

We have developed three approximate methods to compute the current and densities of totally asymmetric exclusion processes involving two internal hopping rates. Additionally, we have simulated the two-rate TASEP and have explored its phase diagram. We find that the dual-rate TASEP retains the three phases found in the standard TASEP model. Within each of these phases the best of our mean field theories provide reliable approximations to the particle currents and densities. In particular, a maximal current phase mean field theory was developed that provides accurate estimates [Eq. (8)] for the current and the density [Figs. 2(a) and 4] in the $(\delta=2, T=2)$ case. Similarly, in the boundary limited phases a mean field method was introduced for the $(\delta=2, T=2)$ case [Eqs. (11) and (12)], which produced accurate estimates for the boundary currents, and reasonably accurate estimates for the maximal currents (Fig 3). In addition to the generally inferior simple mean field approach [Eqs. (2), (4), and (6)], we have developed a primarily numerical mean field approach that we have termed the finite segment mean field method (FSMF). This method can rapidly produce accurate estimates for the currents and densities in all three phases of the dual-rate TASEP. However, as shown in Fig. 2(b), an increasing number of periods must be included in the finite segment as the period length T is increased in order to accurately model the dual-rate TASEP.

Finally, we have used the finite segment mean field method and Monte Carlo simulations to briefly investigate TASEPs with alternative arrangements of periodic defects. Specifically, we investigated dual-rate TASEPs where the first defect was located at an arbitrary position δ within the first T sites of the lattice. We found that these dual-rate TASEPs do not possess particle-hole symmetry unless the number of sites in the TASEP lattice equals $mT+2\delta$ for an integer $m \geq 1$. When the particle-hole symmetry condition is not met, the phase diagram of the dual rate TASEP is no longer symmetric about the $\alpha=\beta$ line. Additionally, both Monte Carlo simulations and finite segment mean field methods suggest that in the nonsymmetric case, the value of α^* is determined by the position of the first defect in the TASEP lattice, while the value of β^* is independently determined by the position of the last defect.

ACKNOWLEDGMENTS

G.L. acknowledges support from the Natural Science and Engineering Research Council of Canada. T.C. acknowledges support from the NSF (DMS-0206733), and the NIH (K25AI058672). A.B.K. acknowledges support from the Camille and Henry Dreyfus New Faculty Awards Program (under Grant No. NF-00-056), from the Welch Foundation (under Grant No. C-1559), and from the U.S. National Science Foundation through Grant No. CHE-0237105. The au-

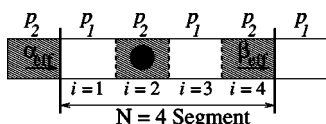


FIG. 11. The arrangement of lattice sites used for an $N=4$ finite segment mean field (FSMF) approximation to the $T=2$ TASEP. The master equation for the state of the four marked lattice sites is solved exactly. The four sites are coupled to the rest of the lattice by assuming an effective injection rate of $\alpha_{\text{eff}}=p_2\sigma_4$ on the left, and an effective extraction rate of $\beta_{\text{eff}}=p_2(1-\sigma_1)$ on the right.

thors thank B. Bergersen and G. N. Patey for valuable comments on the manuscript and C. Greif for his assistance with the Arnoldi diagonalization routines.

APPENDIX A: THE FINITE-SEGMENT MEAN FIELD METHOD

Here we give a detailed description of the the finite segment mean field method, and focus on using the method to solve for the currents and densities in the maximal current phase. Consider a finite lattice containing N sites and a whole number of (p_1, p_1, \dots, p_2) periods (Fig. 11). Assuming the bulk densities in the TASEP lattice are periodic and inherit the same periodicity as the movement rates, we define an effective injection rate (α_{eff}) and an effective extraction rate (β_{eff}) for this finite segment. Specifically, we set $\alpha_{\text{eff}}=p_2\sigma_N$ and $\beta_{\text{eff}}=p_2(1-\sigma_1)$. Using these rates and the known values of p_1 and p_2 , we can build the transition matrix for the master equation describing the motion of the particles in the N -site finite segment.

To construct the master equation, define a vector \vec{r} containing the internal hopping rates of the finite segment, and supply an initial guess for the densities σ_1 and σ_N . Specifically, set the i^{th} entry of \vec{r} equal to the hopping rate of the i^{th} lattice site in the finite segment. The hopping rate of the last site in the finite segment however is set to β_{eff} , so that $r_N = \beta_{\text{eff}}$. With the finite segment and the rate vector (\vec{r}) defined, the algorithm to construct the master equation transition matrix is (see Fig. 12) as follows.

(1) *Label the occupancy states of the finite segment.* Label each occupancy state of the finite-segment with a number determined by treating the occupancy of the lattice as an integer value expressed in base-2. For example, an $N=3$ lattice with only the last site filled (i.e., an occupancy of $\{001\}$), is said to be in *state 1*, while the same lattice with the last two sites filled (an occupancy of $\{011\}$) is said to be in *state 3*.

(2) *Separate the states into two groups.* Separate the states labeled in step (1) into two groups; one group containing the states with the leftmost lattice site unoccupied (the *0-states*), and the other group containing the states with the leftmost lattice site occupied (the *1-states*).

(3) *Enumerate the transitions between the 1-states and the 0-states.* The transitions between the 0-states and the 1-states will always occur between the lowest half of the 1-states, and the highest half of the 0-states. For example, in an $N=3$ finite segment, the transitions take state 4 ($\{100\}$) to state 2 ($\{010\}$),

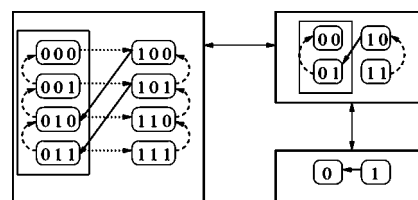


FIG. 12. The steps in the algorithm to generate the transition matrix for a TASEP model. For the purposes of illustration a three site model has been used. Each possible occupancy of the lattice is treated as a bit pattern, and each state is labeled with the corresponding decimal value (i.e., lattice occupancy 011 \rightarrow state 3). The states are divided into two groups: states where the first lattice site is occupied (*1-states*), and states where the first lattice site is empty (*0-states*). Regardless of the number of lattice sites in the TASEP, the transitions between the two classes of states always occur between the first half of the 1-states and the second half of the 0-states (solid arrows). Calling the algorithm recursively on both the 1-states and the 0-states, and ignoring the highest order bit (i.e., the leftmost lattice site), enumerates all the remaining state transitions (dashed arrows). Finally the transitions between each 0-state and each 1-state generated by injection at the left edge of the lattice (dotted arrows) are enumerated.

and state 5 ($\{101\}$) to state 3 ($\{011\}$). To determine the rate of the transitions, we make use of the rate vector \vec{r} . Specifically, we consider the current recursive iteration of the algorithm, and use this as an index for the rate vector. For example, if it is currently the second recursive iteration then all the transitions enumerated involve a particle occupying site 2 moving to site 3. Thus all the transitions occur at rate r_2 ; the rate associated with the second site in the finite segment. In general, the i^{th} recursive iteration of the algorithm will enumerate transitions where a particle occupying site i of the finite segment moves to site $i+1$. These transitions occur at rate r_i .

(4) *Recurse on the 0-states and on the 1-states.* Recurse on the 0-states, and the 1-states, ignoring the leftmost lattice site and starting the recursion from step (2). For example, if on iteration i we are working with an $N=3$ site segment, in iteration $i+1$, we work with *two* $N=2$ site segments. The first of these $N=2$ site segments is generated by ignoring the leftmost lattice site of the 0-states of the $N=3$ segment, while the second $N=2$ site segment is generated by ignoring the leftmost lattice site of the 1-states.

(5) *Enumerate the injection events.* Once the recursion specified in steps (1) through (4) has been completed, enumerate all the transitions representing injections into the finite segment. These transitions take the 0-states to the corresponding 1-states at rate α_{eff} . For example, if we are working on an $N=3$ finite segment, we enumerate the following transitions; $0(\{000\}) \rightarrow 4(\{100\})$, $1(\{001\}) \rightarrow 5(\{101\})$, $2(\{010\}) \rightarrow 6(\{110\})$, and $3(\{011\}) \rightarrow 7(\{111\})$. All these transitions occur at rate α_{eff} .

Using this recursive algorithm to produce the transition matrix for the finite-segment master equation, we can apply an iterative procedure to find the densities and currents through any finite segment of the TASEP lattice. This iterative procedure proceeds as follows.

(1) *Build the master equation.* Given an initial guess for the values of (σ_1, σ_N) , use the recursive algorithm to produce

the transition matrix $[\mathbf{M}(\sigma_1, \sigma_N, p_1, p_2)]$ for the finite-segment master equation. The finite segment densities (σ_1, σ_N) are introduced into \mathbf{M} solely through the effective injection rate $\alpha_{\text{eff}}=p_2\sigma_N$, and the effective extraction rate $\beta_{\text{eff}}=p_2(1-\sigma_1)$.

(2) *Solve the master equation.* To find the steady-state currents and densities, compute the eigenvector $[\vec{V}(\sigma_1, \sigma_2, p_1, p_2)]$ of $\mathbf{M}(\sigma_1, \sigma_N, p_1, p_2)$ associated with the zero eigenvalue

$$M(\sigma_1, \sigma_2, p_1, p_2)\vec{V} = 0. \quad (\text{A1})$$

Normalize \vec{V} using the expression

$$\vec{V} = \frac{\vec{V}}{\sum_i^{2^N} V_i}. \quad (\text{A2})$$

The vector element V_i gives the steady state probability of finding the finite segment in the state with label i . For example, with an $N=3$ finite segment V_3 gives the steady state probability of finding the finite-segment in occupancy state $\{011\}$.

(3) *Compute new density estimates.* With the steady state occupancy probabilities from step (2), compute new estimates for σ_1 and σ_N

$$\begin{aligned} \sigma_1^* &= \sum_{i=2^{N-1}}^{i=2^N-1} V_i, \\ \sigma_N^* &= \sum_{i=1}^{2^{N-1}} V_{2i-1}. \end{aligned} \quad (\text{A3})$$

(4) *Start a new iteration or finish.* Compare the new density estimates (σ_1^*, σ_N^*) , to the previous estimates (σ_1, σ_N) . If $|\sigma_1^* - \sigma_1| \leq \epsilon$ and $|\sigma_N^* - \sigma_N| \leq \epsilon$, then the iteration has reached a fixed point and the procedure ends. Otherwise return to step (1), setting $\sigma_1 = \sigma_1^*$, and $\sigma_N = \sigma_N^*$. Here ϵ is an arbitrary convergence parameter (set to 10^{-4} in this study).

Once a fixed point in the finite-segment densities (σ_1, σ_N) is finally reached, the current through the finite segment can easily be computed from the expression

$$J = \alpha_{\text{eff}}(1 - \sigma_1) = p_2\sigma_N(1 - \sigma_1). \quad (\text{A4})$$

In this appendix we have described an implementation of the finite-segment method useful for generating current and density estimates in the maximal current phase. However, the finite-segment method can be extended to treat the boundary limited phases as well. This can be accomplished by setting $\alpha_{\text{eff}}=\alpha$ or $\beta_{\text{eff}}=\beta$ as appropriate, and applying the density self-consistency condition at the end of the finite-segment that lies in the interior of the TASEP lattice.

While a simple and effective approach, the exponential increase in the size of the transition matrix with the length of the segment quickly renders Eq. (A1) analytically intractable. As a result, Eq. (A1) was solved numerically. Employing the fast Arnoldi-method eigensolvers in the well-known

ARPACK linear-algebra software library [23] and built into the commercial program MATLAB, we could easily treat segments containing ~ 20 lattice sites.

APPENDIX B: CLUSTER MEAN FIELD METHODS

To begin the derivation of the current and density approximations displayed in Eq. (8) consider the pair probability $P(x_i, x_{i+1})$. The pair probability $P(x_i, x_{i+1})$ is the probability of finding a p_1 site with occupancy x_i ($x_i=0$ if lattice site i is empty, $x_i=1$ if lattice site i is occupied), followed by a p_2 site with occupancy x_{i+1} . The time evolution of the occupancy state of any two adjacent sites in a TASEP will depend on the two sites themselves along with the pair of lattice sites immediately to the left or the right of the two site grouping. Thus the master equation for the two site probability $P(0,0)$ is

$$\begin{aligned} \frac{dP(0,0)}{dt} &= -p_2[P(0,1,0,0) + P(1,1,0,0)] \\ &\quad + p_2[P(0,1,0,0) + P(0,1,0,1)]. \end{aligned} \quad (\text{B1})$$

Now assume that each pair of (p_1, p_2) sites behaves like a statistically independent unit, uncorrelated with the other (p_1, p_2) periods in the lattice. Using these assumptions the probabilities in Eq. (B1) can be decomposed into products of pair probabilities, $P(x_i, x_{i+1}, x_{i+2}, x_{i+3}) \approx P(x_i, x_{i+1})P(x_{i+2}, x_{i+3})$. This yields the following equation for $P(0,0)$ in the steady state:

$$\frac{dP(0,0)}{dt} = p_2[P(0,1)^2 - P(0,0)P(1,1)] = 0. \quad (\text{B2})$$

Additionally, by definition

$$\begin{aligned} \sigma_1 &= P(1,0) + P(1,1), \\ \sigma_2 &= P(0,1) + P(1,1), \end{aligned} \quad (\text{B3})$$

$$P(0,0) = 1 - P(0,1) - P(1,0) - P(1,1).$$

Using Eq. (B3) in Eq. (B2), produces the relation

$$P(1,0) = \frac{\sigma_1(1 - \sigma_2) - (\sigma_2 - \sigma_1)^2}{1 + (\sigma_2 - \sigma_1)}. \quad (\text{B4})$$

An equation for $Q(1,0)$, the probability of having an occupied p_2 site followed by an unoccupied p_1 site, can be found from Eq. (B4) by interchanging p_1 and p_2 , as well as σ_1 and σ_2 . Applying the current continuity condition $p_1P(1,0) = p_2Q(1,0)$, results in the relation

$$p_1 \frac{\sigma_1(1 - \sigma_2) - (\sigma_2 - \sigma_1)^2}{1 + (\sigma_2 - \sigma_1)} = p_2 \frac{\sigma_2(1 - \sigma_1) - (\sigma_1 - \sigma_2)^2}{1 + (\sigma_1 - \sigma_2)}. \quad (\text{B5})$$

Now make the substitution $\sigma_2 - \sigma_1 = k$ and define p_1 to be the larger of the two rates. Thus $\sigma_1 < \sigma_2$ and $k > 0$. Solving Eq. (B5) for σ_1 , yields

$$\sigma_1 = \frac{[p_2(1-k^2) - p_1(k-1)^2] + \sqrt{(1-k^2)[k(p_1+p_2) - (p_1-p_2)][3k(p_1+p_2) - (p_1-p_2)]}}{2[k(p_1+p_2) - (p_1-p_2)]}. \quad (\text{B6})$$

Equation (B6) shows that σ_1 is real only when $-1 < k < (p_1-p_2)/3(p_1+p_2)$ or $(p_1-p_2)/(p_1+p_2) < k < 1$. Substituting Eq. (B6) into Eq. (B5) gives $J = kp_1p_2/[(p_1-p_2) - k(p_1+p_2)]$, which shows $J < 0$ for $k > (p_1-p_2)/(p_1+p_2)$, $J > 0$ for $0 < k < (p_1-p_2)/(p_1+p_2)$, and $dJ/dk = p_1p_2(p_1-p_2)/([k(p_2+p_1) + (p_2-p_1)]^2) > 0 \forall k$. Since J must be positive, σ_1 must be real, and J is monotonically increasing with k , the maximum value of the current must occur when $k = (p_1-p_2)/3(p_1+p_2)$. Substituting this value of k into Eq. (B6) yields Eq. (8).

An analogous approach can be used to find current and density estimates in the entry and exit limited regions. Considering the entry limited case first, we find the following master equation for the occupancy of the first two sites in the lattice:

$$\frac{dP(0,0)}{dt} = -\alpha P(0,0) + p_2 P(0,1)[P(0,0) + P(0,1)],$$

$$\begin{aligned} \frac{dP(0,1)}{dt} = & -\alpha P(0,1) - p_2 P(0,1)[P(0,0) + P(0,1)] \\ & + p_1 P(1,0), \end{aligned} \quad (\text{B7})$$

$$\frac{dP(1,0)}{dt} = \alpha P(0,0) + p_2 P(1,1)[P(0,0) + P(0,1)] - p_1 P(1,0),$$

$$\frac{dP(1,1)}{dt} = -p_2 P(1,1)[P(0,0) + P(0,1)] + \alpha P(0,1).$$

Similarly, in the exit limited phase we find the following master equation for the last two sites in the lattice:

$$\frac{dP(0,0)}{dt} = \beta P(0,1) - p_2 P(0,0)[P(0,1) + P(1,1)],$$

$$\begin{aligned} \frac{dP(0,1)}{dt} = & -\beta P(0,1) - p_2 P(0,1)[P(0,1) + P(1,1)] \\ & + p_1 P(1,0), \end{aligned} \quad (\text{B8})$$

$$\frac{dP(1,0)}{dt} = \beta P(1,1) + p_2 P(0,0)[P(0,1) + P(1,1)] - p_1 P(1,0),$$

$$\frac{dP(1,1)}{dt} = -\beta P(1,1) + p_2 P(0,1)[P(0,1) + P(1,1)].$$

Equations (B7) and (B8) assume that the occupancy probabilities $P(x_i, x_{i+1})$ do not vary significantly as a function of position near the entrance and exit of the lattice. This assumption is analogous to that used with the standard TASEP in the boundary limited regions, where the density is assumed to be essentially constant near the rate limiting boundary. Applying the normalization condition on the probabilities $P(x_i, x_{i+1})$ and solving Eqs. (B7) and (B8) generates the results displayed in Eqs. (11) and (12), respectively. We note that Eqs. (11) and (12) are equal to the results of the finite-segment mean field method with $T=2$ and a segment length of $N=2$.

-
- [1] B. Derrida, E. Domany, and D. J. Mukamel, *J. Stat. Phys.* **69**, 667 (1992).
[2] C. T. MacDonald, J. H. Gibbs, and A. C. Pipkin, *Biopolymers* **6**, 1 (1968).
[3] B. Derrida, M. R. Evans, V. Hakim, and V. Pasquier, *J. Phys. A* **26**, 1493 (1993).
[4] B. Derrida, *Phys. Rep.* **301**, 65 (1998).
[5] G. M. Schutz and E. Domany, *J. Stat. Phys.* **72**, 277 (1993).
[6] A. B. Kolomeisky, *J. Phys. A* **31**, 1153 (1998).
[7] L. B. Shaw, R. K. P. Zia, and K. H. Lee, *Phys. Rev. E* **68**, 021910 (2003).
[8] G. Lakatos and T. Chou, *J. Phys. A* **36**, 2027 (2003).
[9] A. B. Kolomeisky, G. M. Schutz, E. B. Kolomeisky, and J. P. Straley, *J. Phys. A* **31**, 6911 (1998).
[10] T. Chou and D. Lohse, *Phys. Rev. Lett.* **82**, 3552 (1999).
[11] M. Schreckenberg, A. Schadschneider, K. Nagel, and N. Ito, *Phys. Rev. E* **51**, 2939 (1995).
[12] T. Nagatani, *J. Phys. A* **26**, 6625 (1993).
[13] S. A. Janowsky and J. L. Lebowitz, *Phys. Rev. A* **45**, 618 (1992).
[14] G. Tripathy and M. Barma, *Phys. Rev. Lett.* **78**, 3039 (1997).
[15] G. Tripathy and M. Barma, *Phys. Rev. E* **58**, 1911 (1998).
[16] K. M. Kolwankar and A. Punnoose, *Phys. Rev. E* **61**, 2453 (2000).
[17] M. Bengrine, A. Benyoussef, H. Ez-Zahraouy, J. Krug, M. Loulidi, and F. Mhirech, *J. Phys. A* **32**, 2527 (1999).
[18] D. Chowdhury and J. S. Wang, *Phys. Rev. E* **65**, 046126 (2002).
[19] P. Garrido, J. Marro, and R. Dickman, *Ann. Phys. (N.Y.)* **199**, 366 (1990).
[20] G. Szabo, A. Szolnoki, and L. Bodocs, *Phys. Rev. A* **44**, 6375 (1991).

- [21] A. B. Bortz, M. H. Kalos, and J. L. Lebowitz, *J. Comput. Phys.* **17**, 10 (1975).
- [22] W. H. Press, S. A. Teukolsky, W. T. Vetterling, and B. P. Flannery, *Numerical Recipes in C*, 2nd ed. (Cambridge University Press, Cambridge, England, 1995).
- [23] R. B. Lehoucq, D. C. Sorensen, and C. Yang, *ARPACK Users' Guide: Solution of Large-Scale Eigenvalue Problems with Implicitly Restarted Arnoldi Methods* (SIAM, Philadelphia, 1998).
- [24] B. Derrida and M. R. Evans, *Nonequilibrium Statistical Mechanics in One Dimension* (Cambridge University Press, Cambridge, England, 1997).
- [25] T. Chou and G. Lakatos, *Phys. Rev. Lett.* **93**, 198101 (2004).